Chinese Chemical Letters 34 (2023) 107253

Contents lists available at ScienceDirect

Chinese Chemical Letters

journal homepage: www.elsevier.com/locate/cclet

Study on catalytic mechanisms of Fe_3O_4-rGO_x in three typical advanced oxidation processes for tetracycline hydrochloride degradation

Heshan Zheng[a], Yunying Hou[a], Shuo Li[a,b,c,**], Jun Ma[a,b], Jun Nan[b,c], Nannan Wang[d,*]

[a] College of Chemistry and Chemical Engineering, Qiqihar University, Qiqihar 161006, China
[b] Urban Water Resources Development and Northern National Engineering Research Center, Harbin 150090, China
[c] School of Environment, Harbin Institute of Technology, Harbin 150090, China
[d] Department of Environmental Engineering, Beijing Institute of Petrochemical Technology, Beijing 102617, China

ARTICLE INFO

Article history:
Received 2 December 2021
Revised 19 January 2022
Accepted 20 February 2022
Available online 23 February 2022

Keywords:
Advanced oxidation progresses
Fe_3O_4
Graphene oxide
Mechanism
Reactive oxygen species

ABSTRACT

This study explored the catalytic mechanism and performance impacted by the materials ratio of Fe_3O_4-GO_x composites in three typical advanced oxidation processes (AOPs) of O_3, peroxodisulfate (PDS) and photo-Fenton processes for tetracycline hydrochloride (TCH) degradation. The ratio of GO in the Fe_3O_4-GO_x composites exhibited different trends of degradation capacity in each AOPs based on different mechanisms. Fe_3O_4-$rGO_{20wt\%}$ exhibited the optimum catalytic performance which enhanced the ozone decomposition efficiency from 33.48% (ozone alone) to 51.83% with the major reactive oxygen species (ROS) of $O_2^{\bullet-}$. In PDS and photo-Fenton processes, Fe_3O_4-$rGO_{5wt\%}$ had the highest catalytic performance in PDS and H_2O_2 decomposition for $SO_4^{\bullet-}$, and $^{\bullet}OH$ generation, respectively. Compared with using PDS alone, PDS decomposition rate and TCH degradation rate could be increased by 5.97 and 1.73 times under Fe_3O_4-$rGO_{5wt\%}$ catalysis. In the photo-Fenton system, Fe_3O_4-$rGO_{5wt\%}$ with the best catalyst performance in H_2O_2 decomposition, and TCH degradation rate increased by 2.02 times compared with blank group. Meantime, the catalytic mechanisms in those systems of that the ROS produced by conversion between Fe^{2+}/Fe^{3+} were also analyzed.

Advanced oxidation processes (AOPs) could produce reactive oxygen species (ROS) of hydroxyl radicals ($^{\bullet}OH$), superoxide radicals ($O_2^{\bullet-}$), and sulfate radicals ($SO_4^{\bullet-}$) that with strong oxidation capacity [1]. $^{\bullet}OH$ has great oxidation power to degrade recalcitrant organic contaminants, which has wide range of sources and can be produced by Fenton, Fenton-like, ozone, photocatalysis and sulfate radical-based AOPs (SR-AOPs) [2]. $O_2^{\bullet-}$ is generated by ozone system, and $SO_4^{\bullet-}$ usually appears in persulfate (including peroxodisulfate (PDS) or peroxomonosulfate (PMS)) system [3]. Various AOPs have been widely studied and applied in wastewater treatment for high effective degradation of toxic and biorefractory organic compounds [4].

To improve their efficiency and solve the drawbacks in practical application of low utilization rate of O_3, high energy consumption for activation of SR-AOPs, and narrow pH limitation of Fenton, *etc.*, it is an urgent need to develop new catalysts. As the advantages of high abundance, non-toxicity, and good interface electron transfer ability of iron, iron-based materials have become commonly used heterogeneous catalyst in AOPs. Jin *et al.* synthesized Cu substituted magnetic Fe_3O_4@FeOOH to degrade ofloxacin in Fenton-like process [5]. Fe_3O_4@hollow@$mSiO_2$ was used as catalyst to degrade sulfadiazine in ultrasound-assisted Fenton-persulfate system [6]. Fe_3O_4@CuO_x hollow ball activated PS can remove 95% of sulfadiazine [7]. Composite materials such as Fe_3O_4 nanoparticles are used in various advanced oxidations, which can quickly remove organic substances in wastewater. However, some catalysts have complex synthesis processes and large ion leaching concentrations, which are prone to metal agglomeration. Graphene oxide (GO) is highly oxidized structure of grapheme, comprises high density of oxygenated functional groups, which can effectively prevent the agglomeration and corrosion of metal oxides, making it commonly used as a support material in composite materials [8,9]. Therefore, loading Fe_3O_4 on GO to form a metal composite as a catalyst for AOPs can effectively degrade pollutants. rGO/Fe nanoparticles were used as adsorbents and Fenton-like catalysts to remove 93.6% of

* Corresponding author.
** Corresponding author at: College of Chemistry and Chemical Engineering, Qiqihar University, Qiqihar 161006, China
E-mail addresses: shuo_105@163.com (S. Li), wnn_flying@163.com (N. Wang).

https://doi.org/10.1016/j.cclet.2022.02.058
1001-8417/

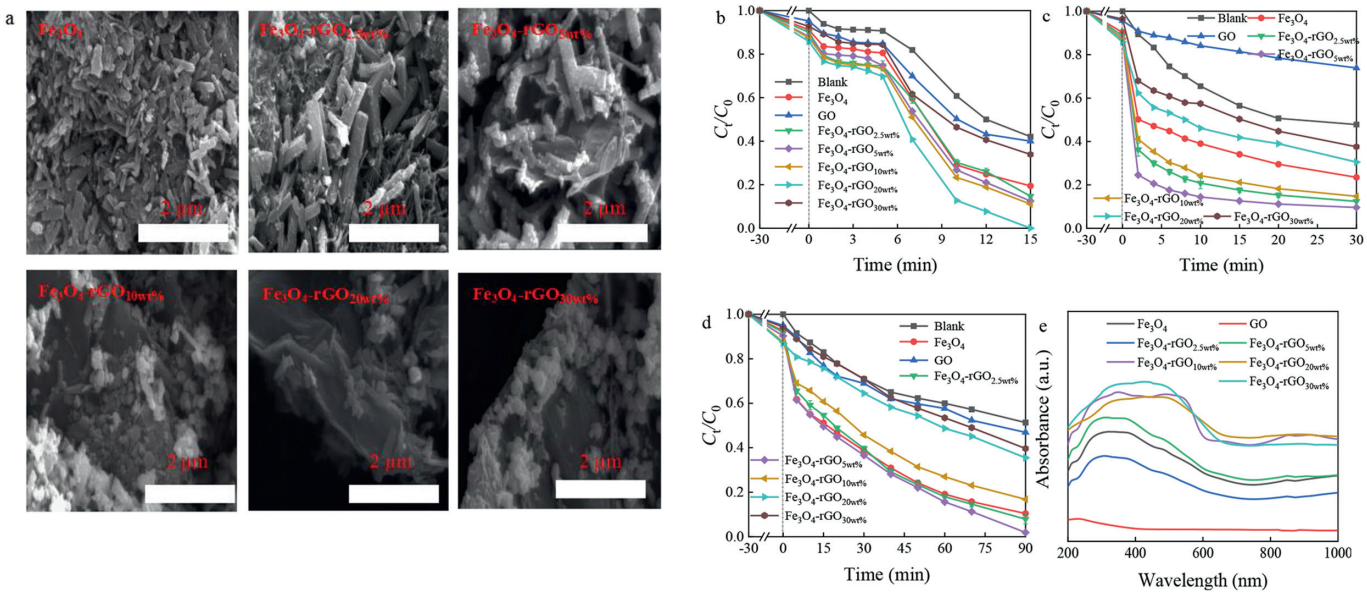

Fig. 1. (a) SEM images of pure Fe_3O_4 and Fe_3O_4-rGO_x samples. Catalytic degradation of TCH in (b) O_3 system, (c) PDS system; (d) photo-Fenton progress. (e) UV-vis diffuse reflectance spectrum of pure Fe_3O_4 and Fe_3O_4-rGO_x samples (Reaction conditions: [TCH] = 60 mg/L, [O_3] = 4.0 mg/min, [PDS] = 0.1 g, the temperature of PDS system = 60 °C, [H_2O_2] = 0.2 mol/L, [UV] = 200–400 nm, [catalysts] = 0.5 g/L, pH 4.6).

mitoxantrone from the wastewater [10]. NGO/Fe_3O_4 was used as a catalyst to activate potassium persulfate to degrade norfloxacin under the assistance of ultraviolet light [11]. GO-Fe_3O_4 nanocomposites was used as catalyst for degradation of ofloxacin by pulsed discharge plasma [12].

Although it is reported that Fe_3O_4-GO_x as a catalyst enhances the degradation of certain organic pollutants in AOPs, the mechanism of its catalytic degradation of pollutants is lack of in-depth analysis. Tetracycline hydrochloride (TCH) as a broad-spectrum antibiotic is widely used as an antibacterial agent and feed additive, thereby we chose it as the target pollutant. Therefore, we studied the catalytic mechanisms of Fe_3O_4-GO_x synergistically catalyzed oxidants decomposition and pollutant degradation in AOPs (including ozonation, persulfate catalysis and photo-Fenton progress) that based on different free radicals. In this paper, (i) the effect of GO loading ratio on the morphology of the composites was analyzed by characterization; (ii) the effects of different proportions of Fe_3O_4 and GO on the degradation efficiency of TCH in three AOPs were systematically analyzed; (iii) the potential mechanism of TCH degradation of the composites were clarified by detecting the oxidant concentration in the solution, and utilizing X-ray photoelectron spectroscopy (XPS), quenching experiment and electron spin resonance (ESR).

According to the published paper, using solvothermal process synthesized Fe_3O_4 and Fe_3O_4-rGO_x (Text S1 in Supporting information) [12]. The morphology of Fe_3O_4 and Fe_3O_4-rGO_x were observed by SEM, which were shown in Fig. 1a. Fe_3O_4 exhibited irregular rob shape, after loading Fe_3O_4 on the GO layer, the particle size of Fe_3O_4 gradually decreased as the amount of GO increased. This may be that the GO surfaces contain negatively charged oxygen-containing groups which could be adsorbed on the broadside of Fe_3O_4 crystals, and imposed a certain strain on them, thus limiting the growth of Fe_3O_4 [13]. Meantime, with the increase of GO content, the main crystal surface of Fe nanoparticles was affected, which made the larger crystal surface was replaced by the smaller crystal surface [12]. Fig. S1a (Supporting information) was the X-ray diffraction (XRD) patterns of GO, Fe_3O_4 and Fe_3O_4-rGO_x. In the GO spectrum, an evident peak at 2θ = 11.2° was consistent with previous research [12,14]. The peaks of Fe_3O_4 and Fe_3O_4-rGO_x located at 30.1°, 35.5°, 43.3°, 53.6°, 57.2° and 62.7° were accordance with the (220), (311), (400), (422), (511) and (440) crystal faces of Fe_3O_4 [15]. Moreover, the characteristic peaks of rGO were observed at 21.2° and 26° in Fe_3O_4-rGO_x composites, indicating that GO had been reduced to rGO, which also demonstrated the successful synthesis of composites [16]. Fig. S1b (Supporting information) displayed the FT-IR patterns of Fe_3O_4 and Fe_3O_4-rGO_x. The absorbed H_2O molecule or surface hydroxyl were detected the range of 3000–3500 cm^{-1} [17]. The $-CH_2-$ was observed at 2800–2900 cm^{-1} in Fe_3O_4-rGO_x, and the peak shifted from 1633 to 1600 cm^{-1} because of GO doping to form $-COO-$ [3]. Besides, all samples had an obvious absorption peak at 570 cm^{-1}, which was the Fe−O−Fe stretching vibration [18].

Figs. 1b–e depicted degradation rate of TCH with different ratio of Fe_3O_4 to GO_x in AOPs. All catalysts did not significantly adsorb TCH during 30 min, indicating that catalytic oxidation dominated the removal of TCH. The adsorption efficiency also increased with the increase of GO loading. However, when the GO loading increased to 30 wt%, the adsorption efficiency was only 3.6%. The reason was that GO folding each other lead to a reduction in the size and number of pores. The salient features and trends in TCH degradation in AOPs, as evident from the results were presented in Fig. 1. In Fig. 1b, the degradation rate was limited by the ozone dissolution in catalytic ozonation stages. After 5 min of treatment, the efficiency of O_3 to remove TCH alone was 9.31%, and it reached 57.93% after 15 min. After adding Fe_3O_4, the removal efficiency of TCH increased to 80.55%. Compared with Fe_3O_4, Fe_3O_4-rGO_x enhanced the removal efficiency of TCH clearly. Because strong interaction between Fe_3O_4 and GO could decompose O_3 to produce $O_2^{\bullet-}$ and H_2O_2, and then H_2O_2 reacted with O_3 to produce $^{\bullet}OH$ [19,20]. Meantime, GO acted as a carrier to disperse the active sites on its surface and expanded the contact area between oxidants and contaminants. Fig. S2a (Supporting information) showed the transient photocurrent response of pure Fe_3O_4 and Fe_3O_4-rGO_x. Compared with Fe_3O_4, Fe_3O_4-rGO_x composites exhibited a significantly enhanced photocurrent density, which indicated that the electron transfer was promoted between Fe_3O_4 and rGO. Meantime, the higher photocurrent response of the sample was, the more effective separation of the photoelectron-hole pairs will be obtained, which evidenced that Fe_3O_4-$rGO_{20wt\%}$ composite that with the

most efficient separation were due to the strongest photocurrent response. Therefore, with the increased of GO content, the removal rate of TCH also increased. The degradation efficiency of TCH by the Fe_3O_4-$rGO_{20wt\%}$ was 100% and the reaction rate constant (k_2) was 0.017 g mg^{-1} min^{-1} and higher than that derived from other catalysts (the k_2 of other catalysts were 0.004, 0.005, 0.005, 0.006 and 0.002 g mg^{-1} min^{-1}) (Text S2, Fig. S1c and Table S1 in Supporting information).

As illustrated in Fig. 1c, the removal of TCH was observed about 52.17% in the blank group during 30 min reaction time, which may be attributed that PDS under the heating condition produced ROS to degrade TCH. Fe_3O_4 and GO activating PDS systems had only 76.51% and 26.13% removal ratio of TCH, respectively. Under the support of GO, the catalytic performance of Fe_3O_4-rGO_x was remarkably improved. From Fig. S1d and Table S1 (Supporting information), TCH had a highest rate constant of 0.0052 g mg^{-1} min^{-1} ($R^2 = 0.954$) in Fe_3O_4-$rGO_{5wt\%}$/PDS system, approximately 1.3 times than that of Fe_3O_4/PDS system. The raised degradation efficiency was obviously ascribed to the increase of available active sites for PDS decomposition. When GO loading was 2.5 wt%, 10 wt%, 20 wt% and 30 wt%, TCH removal rate and k_2 were both reduced. This was mainly attributable to the enhancement of free radicals scavenging effect of reactive sites on Fe_3O_4-rGO_x surface, meantime, acidic conditions will limite the produce of $^{\bullet}OH$ [21].

In photo-Fenton system, as was displayed in Fig. 1d, TCH degradation efficiency was less than 50% after 90 min without catalyst. However, the degradation rate of pure Fe_3O_4 to TCH was 90.60%, which was close to that of Fe_3O_4-$rGO_{5wt\%}$ to TCH (98.11%). Therefore, a pseudo-first-order model was used to compare the catalytic activity of the two catalysts. In Fig. S1e and Table S1 (Supporting information), the rate constant of Fe_3O_4-$rGO_{5wt\%}$ was 1.5 times that of Fe_3O_4, so the catalytic activity of Fe_3O_4-$rGO_{5wt\%}$ was better than Fe_3O_4. From the UV-vis diffuse reflectance spectrum of pure Fe_3O_4 and GO, Fe_3O_4-rGO_x composites, which can be seen that the optical properties of materials. Fig. 1e showed that the Fe_3O_4-rGO_x composites exhibited stronger absorption throughout visible light range than Fe_3O_4 and GO. This may be attributed to the specific structure: GO sheets and Fe_3O_4 particles allowed multiple reflections of light. According to the study of Moztahida *et al.* [15], and the results of UV-vis diffuse reflectance spectrum and photocurrent (Fig. 1e and Fig. S2a in Supporting information) also showed that the addition of rGO increased the light adsorption capacity of Fe_3O_4-rGO_x composites and provided more electrons and holes (h^+) for the production of ROS. However, by GO loading ratio from 5 wt% to 30 wt% increasing, its removal efficiency was diminished from 98.11% to 60.37%. Because the increase of GO loading affected the turbidity of solution, which lead the increase of the resistance of UV to penetrate it and shielded light adsorption [22], even affected charge separation [15]. Hence, the Fe_3O_4-$rGO_{5wt\%}$ had the optimum catalytic performance.

To investigate the potential for recycling of catalysts, the tetracycline oxidation testing was performed in 5 cycles in three AOPs, respectively. As could be seen from Fig. S2b (Supporting information), the removal efficiency of the TCH gradually decreased with the increase of the number of times of use. The removal rate of about 80% indicated that materials were stable and had a certain reusability. Compared with the 1st run, TCH degradation rate decreased slightly in the 5th, which might be due to the surface oxidation of the catalyst and leaching of metal ions during the catalytic process [20]. The leaching rate of metal ions was shown in Table S2 (Supporting information). And the leaching amount of total iron and Fe^{2+} was less than 0.1% with respect to the catalyst dose of 500 mg/L. However, the temperature condition of PDS system was 60 °C (O_3 and photo-Fenton systems were carried out at room temperature), which lead the increase of ion leaching rate of catalysts. In addition, the leached Fe concentration at the end of each round almost kept the same level, which satisfied the water environment discharge standards (2 mg/L) imposed by the European Union [23].

The proportion of GO in Fe_3O_4-rGO_x affected TCH degradation in the three AOPs. Therefore, we conducted a series of experiments to explore the effect of GO loading ratio on TCH degradation and the mechanism of catalysts in AOPs. Fig. 1a showed that GO_x affected the morphology of catalyst, and further effected TCH degradation (Fig. 1b). To verify that catalysts enhanced O_3 decomposition, this experiment measured the ozone concentra-

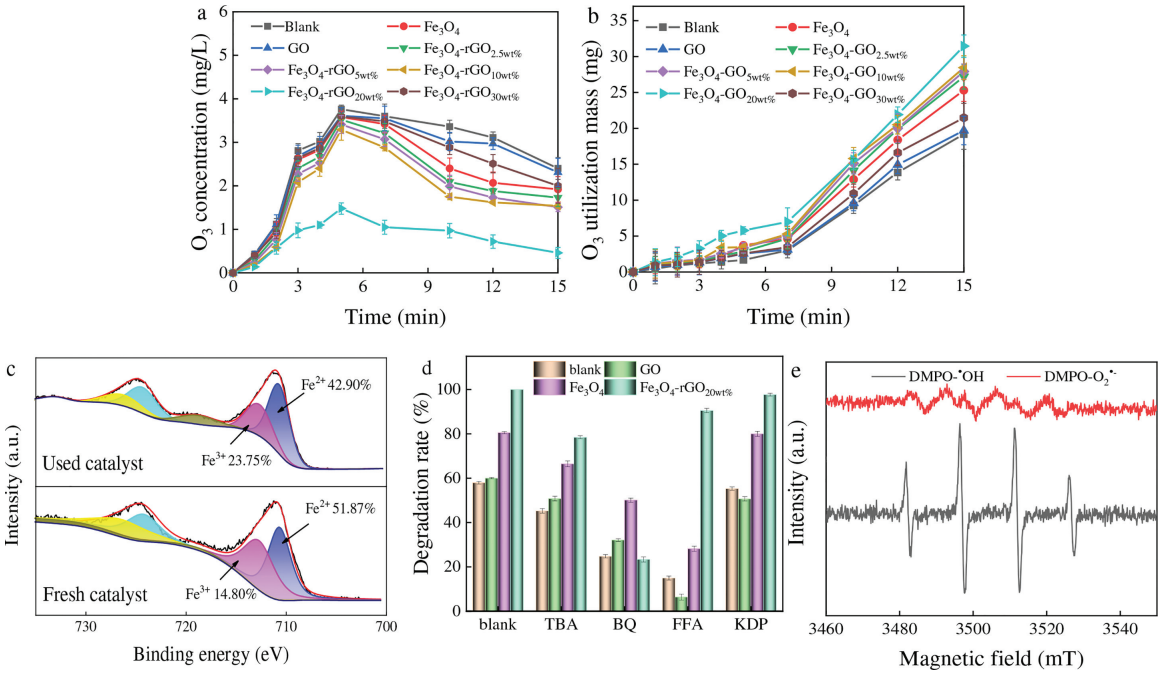

Fig. 2. (a) Ozone concentration and (b) ozone utilization mass in solution. (c) XPS spectra for Fe 2p regions of fresh and used Fe_3O_4-$rGO_{20wt\%}$ in O_3 system. (d) Effects degradation efficiency of TCH with the presence of quenchers. (e) ESR spectra detected in Fe_3O_4-$rGO_{20wt\%}$/O_3 systems for DMPO-$^{\bullet}OH$ and DMPO-$O_2^{\bullet-}$ (Reaction conditions: [TCH] = 60 mg/L, [O_3] = 4.0 mg/min, [catalysts] = 0.5 g/L, pH 4.6).

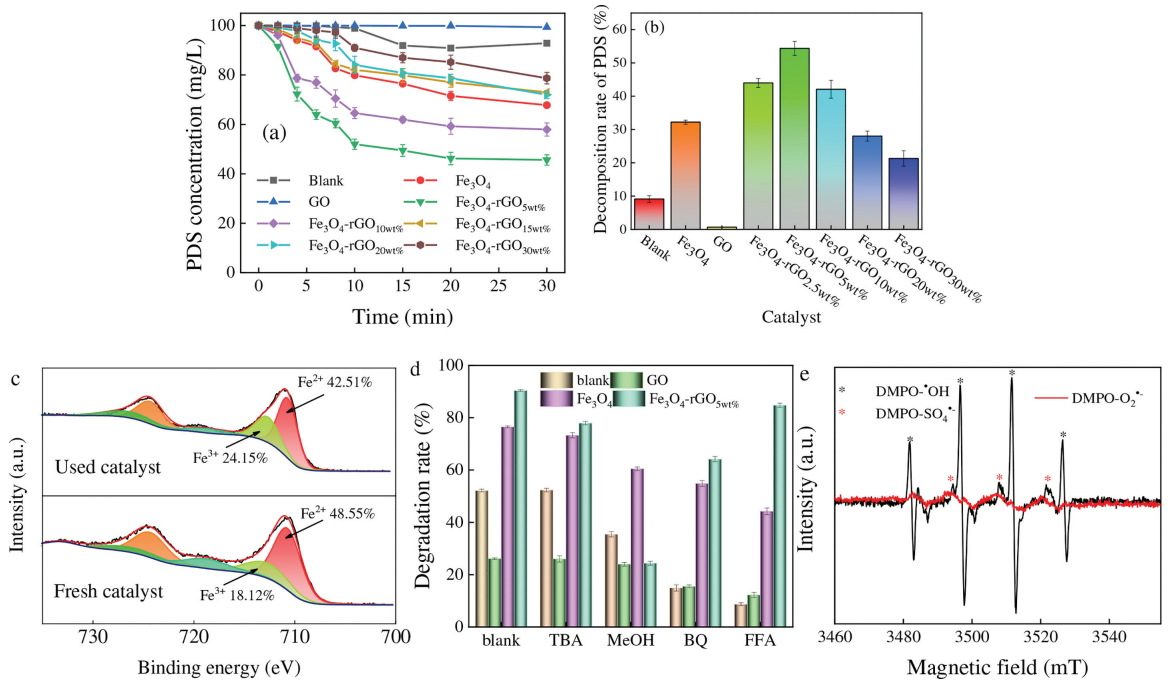

Fig. 3. (a) PDS concentration in solution and (b) PDS decomposition rate. (c) XPS spectra for Fe 2p regions of fresh and used Fe_3O_4-$rGO_{5wt\%}$ in PDS system. (d) Effects degradation efficiency of TCH with the presence of quenchers. (e) ESR spectra detected in Fe_3O_4-$rGO_{5wt\%}$/PDS system for DMPO-•OH, DMPO-$SO_4^{\bullet-}$ and DMPO-$O_2^{\bullet-}$ (Reaction conditions: [TCH] = 60 mg/L, [PDS] = 0.1 g, the temperature of PDS system = 60 °C, [catalysts] = 0.5 g/L, pH 4.6).

tion in liquid phase of each system, and the test results were shown in Fig. 2a. The ozone concentration in the solution gradually rose within 5 min, because ozone undergo a mass transfer process from the gas phase to the liquid phase [24,25], and TCH degradation hardly changed within 5 min. The concentration of liquid phase ozone reached 3.76 mg in 5 min in blank group, and then remained stable; after adding Fe_3O_4, the ozone concentration reached 3.58 mg/L in 5 min, and Fe_3O_4-$rGO_{20wt\%}$/O_3 system reached 1.48 mg/L in 5 min (other catalysts system reached about 3.5 mg/L), and the solution ozone concentration finally reached 2.4, 1.33, 2.31, 1.73, 1.71, 1.54, 0.46 and 2.09 mg/L, respectively. It indicated that the catalyst can accelerate ozone decomposition, reduce solution ozone concentration, and thereby improve the utilization mass of ozone. Eq. S3 (Text S3 in Supporting information) was used to calculate the ozone utilization mass to better show the mechanism of Fe_3O_4-GO_x/O_3 system [26].

The ozone utilization mass was shown in Fig. 2b. According to Eq. S3, it under those systems was 19.19, 25.31, 19.70, 27.2, 27.92, 28.46, 31.45 and 21.47 mg, respectively. Compared with control groups, Fe_3O_4-rGO_x enhanced TCH degradation and O_3 utilization mass clearly. The reason was that strong interaction between Fe_3O_4 and GO_x could decompose O_3 to produce $O_2^{\bullet-}$ and H_2O_2, and then H_2O_2 reacted with O_3 to produce •OH (Text S4 and Eqs. S4-S13 in Supporting information) [19,20]. Fig. 2c was XPS spectra of Fe 2p before and after Fe_3O_4-$rGO_{20wt\%}$, which corroborated the Fe^{2+}/Fe^{3+} species participated in the electron-transfer processes and contributed to the utilization of ozone (Fe^{2+} changed from 51.87% to 42.90%). The fitting peaks at the binding energies of 710.7 and 724.3 eV belong to Fe^{2+}, while the fitting peaks at the binding energies of 712.7 and 726.3 eV were Fe^{3+} [27,28]. To explore ROS in O_3 system, *tert*–butanol (TBA), benzoquinone (BQ), furfuryl alcohol (FFA) and phosphate (KDP) were added in solution to quench •OH, $O_2^{\bullet-}$, $^1O_2$ and surface of •OH, respectively Fig. 2d displayed the major ROS in ozone system. After BQ injected, all the $O_2^{\bullet-}$ generated in Fe_3O_4-$rGO_{20wt\%}$/O_3 system was nearly quenched and resulting in a decrease in TCH removal from 100% (without quencher) to 23.35%. The addition of TBA, FFA and KDP reduced the TCH removal rate to 78.46%., 90.52%. and 97.31%. Therefore, it was deduced that $O_2^{\bullet-}$ was the main reactive oxygen species generated in the Fe_3O_4-$rGO_{20wt\%}$/O_3 system, •OH and $^1O_2$ had no significant effects in the catalytic ozone system. However, $^1O_2$ and $O_2^{\bullet-}$ were the major ROS in GO and Fe_3O_4 system. ESR measurements were carried out to further accurately elucidate the existence of ROS in Fe_3O_4-$rGO_{20wt\%}$/O_3 system (Fig. 2e). The $O_2^{\bullet-}$ and •OH signals can be observed in the Fe_3O_4-$rGO_{20wt\%}$/O_3 process in Fig. 2e indicated that Fe_3O_4-$rGO_{20wt\%}$ can decompose ozone to generate $O_2^{\bullet-}$ and •OH.

As shown in Fig. 1c, PDS as the main oxidant participating of Fe_3O_4-rGO_x/PDS process played an important role. In order to explore catalytic mechanism in system, PDS concentration and decomposition rate were measured and concluded in solution. It can be seen in Figs. 3a and b, PDS decomposition increased with the decreased concentration of that in solution. Comparing with other catalysts, Fe_3O_4-$rGO_{5wt\%}$ had the lowest PDS concentration (45.63 mg/L) and the highest PDS decomposition rate (54.37%). Therefore, Fe_3O_4-$rGO_{5wt\%}$ had the highest TCH degradation in PDS system. As exhibited in Fig. 3c, compared with fresh Fe_3O_4-$rGO_{5wt\%}$, it was found that the peak area of Fe^{2+} decreases and Fe^{3+} increased after reaction, which indicated that the transition between Fe^{2+} and Fe^{3+} during the reaction activated the decomposition of PDS to produce ROS. Therefore, to further explore the mechanism for Fe_3O_4-$rGO_{5wt\%}$, we analyzed the type of ROS in this system. It was reported that $SO_4^{\bullet-}$ and •OH could be produced by the metal-based catalysts activated PDS [29,30]. As given in Fig. 3d, the TCH degradation efficiency decreased from 90.4% to 24.38% and 57.3% with addition of methanol (MeOH) and TBA, respectively. And adding BQ, the removal rate of TCH decreased to 64.16%. This result clearly indicated that the degradation process was a pure radical-based oxidation process. Moreover, both $SO_4^{\bullet-}$ and •OH occurred in the Fe_3O_4-$rGO_{5wt\%}$/PDS system and the latter one played a much more important role. Similarly, Chen *et al.* [30] claimed that the sulfate radical was the dominating radical species responsible for the degradation of norfloxacin by $CoFe_2O_4$-GO/PMS system. However, Fig. 3d results revealed that $^1O_2$, $O_2^{\bullet-}$

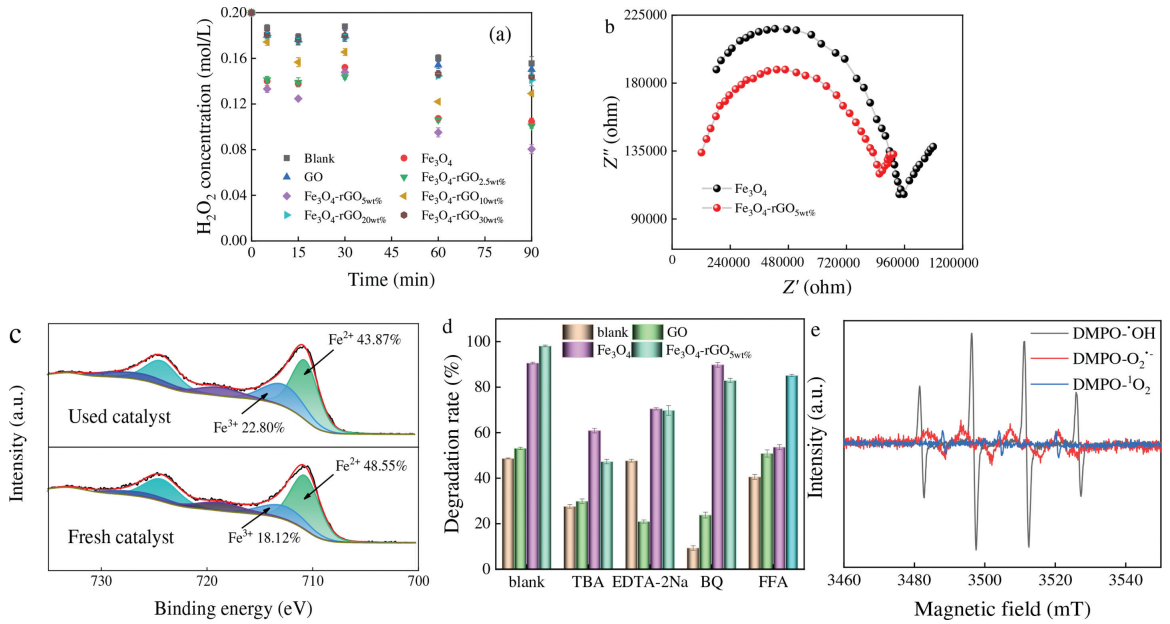

Fig. 4. (a) H_2O_2 concentration in photo-Fenton system. (b) EIS Nyquist plots of Fe_3O_4 and Fe_3O_4-$rGO_{5wt\%}$. (c) XPS spectra for Fe 2p regions of fresh and used Fe_3O_4-$rGO_{5wt\%}$ in PDS system. (d) Effects degradation efficiency of TCH with the presence of quenchers. (e) ESR spectra detected in Fe_3O_4-$rGO_{5wt\%}$/UV/H_2O_2 system for DMPO-·OH, DMPO-$O_2^{\bullet-}$ and DMPO-$^1O_2$ (Reaction conditions: [TCH] = 60 mg/L, [H_2O_2] = 0.2 mol/L, [UV] = 200–400 nm, [catalysts] = 0.5 g/L, pH 4.6).

and $SO_4^{\bullet-}$ were generated in PDS, GO/PDS and Fe_3O_4/PDS system, in which $^1O_2$ and $O_2^{\bullet-}$ were the dominant ROS [15]. Therefore, PDS itself will produce a small amount of ROS to degrade TCH at 60 °C. Meantime, in a review about the treatment of wastewater by the sulfate-based AOPs, Fang *et al.* [31] have analyzed that $SO_4^{\bullet-}$ dominate the acidic pH conditions. According to study of Wang *et al.* [32] and Jing *et al.* [3], a possible mechanism for PDS activation by Fe_3O_4-$rGO_{5wt\%}$ was proposed (Eqs. S14-S26 shown in Supporting information Text S5). ESR signals of ·OH, $SO_4^{\bullet-}$ and $O_2^{\bullet-}$ were observed in the system (Fig. 3e), the results confirmed the previous inference that $SO_4^{\bullet-}$, $O_2^{\bullet-}$ and ·OH existed in Fe_3O_4-$rGO_{5wt\%}$/PDS system. The increase of GO loading ratio expanded the reaction site and produced a large amount of ROS. However, excessive $SO_4^{\bullet-}$ will quench each other. Therefore, Fe_3O_4-$rGO_{5wt\%}$ had the best catalytic performance compared with others.

About the difference of TCH degradation in photo-Fenton progress, it was speculated that increase of GO loading lead the turbidity of solution increased, which made high resistance for light to penetrate solution, decreased H_2O_2 decomposition and further affected TCH degradation. To verify this hypothesis, the influences of those catalysts were tested on the concentration of H_2O_2. In Fig. 4a, the H_2O_2 concentration of blank, Fe_3O_4, GO and Fe_3O_4-rGO_x were 155.62, 104.53, 150.24, 100.77, 80.42, 129.41, 141.07 and 143.85 mg/L, which suggested that GO loading ratio affected H_2O_2 decomposition and TCH degradation. Compared with other systems, Fe_3O_4-$rGO_{5wt\%}$/UV-H_2O_2 system had the lowest H_2O_2 concentration. Moreover, using Fig. 4b analyzed the interfacial charge transfer capabilities of Fe_3O_4 and Fe_3O_4-$rGO_{5wt\%}$. The arc radius of the Nyquist curve for Fe_3O_4-$rGO_{5wt\%}$ was significantly smaller than that of Fe_3O_4, which implied that the charge of the Fe_3O_4-$rGO_{5wt\%}$ at the interface migration resistance decreased and the e^- mobility of the composite was enhanced. As shown in Fig. 4c, supported by the fitting parameters, that of Fe^{2+} and Fe^{3+} for the pristine Fe_3O_4-$rGO_{5wt\%}$ were 48.55% and 18.12%, respectively. After the degradation reactions, the peak area of Fe^{2+} slumped to 43.87%, while the peak area ratio of Fe^{3+} went up to 22.80%, which suggested that Fe^{2+}/Fe^{3+} were involved in electron transfer processes. And Fig. 4d illustrated ·OH and h^+ were the main ROS in Fe_3O_4-$rGO_{5wt\%}$/UV/H_2O_2 system (ethylenediamine tetraacetic acid disodium (EDTA-2Na) quenched h^+), $O_2^{\bullet-}$, ·OH and h^+ existed in GO and Fe_3O_4 system, and the major ROS of blank group were $O_2^{\bullet-}$ and ·OH (corresponding degradation mechanism was shown in Eqs. S27-S34 and Text S6 in Supporting information) [15,33]. As shown in Fig. 4e, characteristic ESR signals of ·OH, $O_2^{\bullet-}$ and $^1O_2$ can be observed in the catalytic system of Fe_3O_4-$rGO_{5wt\%}$/UV/H_2O_2, thus ·OH, $O_2^{\bullet-}$ and $^1O_2$ were existed in this system. Meantime, researchers also observed the similar conclusion in the removal of sulfamethoxazole in the Fe_3S_4 derived from MIL-100(Fe)/Vis/H_2O_2 system.

In order to understand the source of $O_2^{\bullet-}$ in three AOPs, nitrogen bubble was blown into the solution to further verify and revealed degradation mechanism. In Fig. S3 (Supporting information), the degradation rate of TCH in PDS system was 72.96%. Compared with no N_2, that of TCH decreased by 17.44%. However, in Fig. 3d, the inhibition rate of TCH after adding BQ was 26.24%, which indicated that the formation of $O_2^{\bullet-}$ in PDS system was attributed in dissolved oxygen in solution and the decomposition of water molecules. However, none of the other systems were affected, which indicated that $O_2^{\bullet-}$ all came from the reaction between catalyst and substances in systems. And among these three AOPs, O_3 system completely removed TCH within 15 min, which is far superior to the PDS and photo-Fenton systems. Therefore, O_3 system is an effective technology to treat TCH wastewater.

In conclusion, the content of GO in Fe_3O_4-rGO_x composites greatly affected the performance and mechanism of TCH degradation in three typical AOPs. In O_3 system, Fe_3O_4-$rGO_{20wt\%}$ exhibited the best catalytic efficiency which could increase the degradation rate of TCH from 57.93% (only O_3) to 100%. The results showed that the strong force between Fe_3O_4 and rGO also improved the decomposition rate of O_3 by Fe_3O_4-$rGO_{20wt\%}$, and the conversion between Fe^{2+} and Fe^{3+} decomposed oxidant and produced $O_2^{\bullet-}$ and ·OH to degrade TCH that detected by ESR spectra. For PDS oxidation system, Fe_3O_4-$rGO_{5wt\%}$ showed higher catalytic activity compared with others By detecting the concentration of PDS in the solution, quenching experiment and ESR analysis found that Fe_3O_4-$rGO_{5wt\%}$ can effectively decompose PDS and produce $SO_4^{\bullet-}$ and $O_2^{\bullet-}$, and PDS decomposition rate and TCH degradation rate were 5.97 and 1.73 times higher than those of the blank group. In the photo-Fenton system, the rate of H_2O_2 decomposition by Fe_3O_4-$rGO_{5wt\%}$ was higher than that of others. Meantime, the addition of

rGO enhanced the corresponding light region of the composite and separation of photogenerated electron-holes. However, increased GO ratio also enhanced the turbidity of the solution and shielded UV. Therefore, though Fe_3O_4-$rGO_{10wt\%}$-Fe_3O_4-$rGO_{30wt\%}$ with higher photocurrent density, Fe_3O_4-$rGO_{5wt\%}$ exhibited a higher rate of TCH degradation in UV-H_2O_2 system. In this system, multiple reactive species including $^{\bullet}OH$, $O_2^{\bullet-}$ and $^1O_2$ were detected that responsible for the TCH degradation.

Declaration of competing interest

All authors declared that they do not have any commercial and associative interests that represent a conflict of interest in connection with the other work submitted.

Acknowledgments

The work was supported by the National Natural Science Foundation of China (Nos. 21906088, 51902169, 52170039), the National Science Foundation for Post-doctoral Scientists of China (No. 2021T140165), the Natural Science Foundation of Heilongjiang Province, China (No. LH2020B023), Department of Education Heilongjiang Province (No. 135309338), University Nursing Program for Young Scholars with Creative Talents in Heilongjiang Province (Nos. UNPYSCT-2020068, UNPYSCT-2020067), the authors also gratefully acknowledge the financial support by the Heilongjiang Provincial Key Laboratory of Surface Active Agent and Auxiliary (No. BMHXJKF009).

Supplementary materials

Supplementary material associated with this article can be found, in the online version, at doi:10.1016/j.cclet.2022.02.058.

References

[1] T. Xia, Y. Lin, W. Li, M. Ju, Chin. Chem. Lett. 32 (2021) 2975–2987.
[2] X. Feng, H. Guo, K. Patel, H. Zhou, X. Lou, Chem. Eng. J. 244 (2014) 327–334.
[3] J.N. Jing, C.J. Cao, S.J. Ma, et al., Chem. Eng. J. 407 (2021) 126890.
[4] Y. Zhang, J.B. Zhou, X. Chen, et al., Chem. Eng. J. 369 (2019) 745–757.
[5] J. Hang, X. Tian, Y. Nie, et al., Environ. Sci. Technol. 51 (2017) 12699–12706.
[6] K. Roy, V.S. Moholkar, Chem. Eng. J. 386 (2020) 121294.
[7] T. Liu, K. Wu, M. Wang, et al., Chemosphere 262 (2021) 127845.
[8] L.L. Kong, L.Y. Fan, Chin. Chem. Lett. 27 (2016) 827–831.
[9] Y. Su, M. Lu, R. Su, et al., Chin. Chem. Lett. 33 (2022) 2573–2578.
[10] J. Wu, M. Lin, X.L. Weng, et al., Chem. Eng. J. 408 (2021) 127273.
[11] J. Wu, J. Bai, Z. Wang, et al., Environ. Technol. 43 (2022) 95–106.
[12] H. Guo, Z. Li, S.Y. Lin, et al., Chemosphere 265 (2021) 129089.
[13] Z. Ren, E. Kim, S.W. Pattinson, et al., Chem. Sci. 3 (2012) 209–216.
[14] F. Görmez, O. Görmez, B. Görmez, et al., J. Environ. Chem. Eng. 7 (2019) 102990.
[15] M. Mortahida, J. Jang, M. Nawaz, S.R. Lim, D.S. Lee, Sci. Total Environ. 667 (2019) 741–750.
[16] J. Wang, F. Yang, S. Wang, et al., J. Taiwan Inst. Chem. Eng. 99 (2019) 113–122.
[17] H. Fan, G. Yi, X. Zhang, et al., Opt. Mater. 111 (2021) 110582.
[18] X. Wang, B. Guo, W. Fu, H. Yang, J. Water Process Eng. 31 (2019) 100814.
[19] J. Nawrocki, B. Kasprzyk-Hordern, Appl. Catal. B: Environ. 99 (2010) 27–42.
[20] L. Jothinathan, J.Y. Hu, Water Res. 134 (2018) 63–73.
[21] X.W. Zhang, F. Wang, C.C. Wang, et al., Chem. Eng. J. 426 (2021) 131927.
[22] Y. Gong, X. Zhao, H. Zhang, et al., Appl. Catal. B: Environ. 233 (2018) 35–45.
[23] Q.S. Wu, H.P. Yang, L. Kang, et al., Appl. Catal. B: Environ. 263 (2020) 118282.
[24] H. Chen, J.L. Wang, J. Hazard. Mater. 403 (2021) 123697.
[25] D. Zheng, J. Cao, P. Wang, J. Zhao, C. Li, Environ. Technol. 42 (2020) 1–21.
[26] H. Chen, J.L. Wang, Chemosphere 234 (2019) 14–24.
[27] M. Chen, N. Wang, X. Wang, Y. Zhou, L. Zhu, Chem. Eng. J. 413 (2021) 127539.
[28] L. Yang, C.S. Chen, Y.J. Tu, Y.H. Huang, Z. Hui, Environ. Sci. Technol. 49 (2015) 6838–6845.
[29] L. Lei, X. Hao, X. Zhang, M. Zhou, Plasma Process Polym. 4 (2007) 455–462.
[30] S. Giannakis, K.Y.A. Lin, F. Ghanbari, Chem. Eng. J. 406 (2021) 127083.
[31] G.D. Fang, D.D. Dionysiou, Y. Wang, et al., J. Hazard. Mater. 227-228 (2012) 394–401.
[32] H.X. Wang, W. Rong, S.H. Wei, et al., Chin. Chem. Lett. 27 (2016) 1572–1576.
[33] J. Hang, X.H. Yi, C.C. Wang, et al., J. Hazard. Mater. 424 (2022) 127415.